Telecom-wavelength single-photon sources for quantum communications

2007 J. Phys.: Condens. Matter 19 225005

(http://iopscience.iop.org/0953-8984/19/22/225005)

IOP PUBLISHING JOURNAL OF PHYSICS: CONDENSED MATTER

J. Phys.: Condens. Matter **19** (2007) 225005 (14pp) doi:10.1088/0953-8984/19/22/225005

Telecom-wavelength single-photon sources for quantum communications

A Fiore[1,2], C Zinoni[1], B Alloing[1], C Monat[1], L Balet[1], L H Li[1], N Le Thomas[1], R Houdré[1], L Lunghi[2], M Francardi[2], A Gerardino[2] and G Patriarche[3]

[1] Ecole Polytechnique Fédérale de Lausanne, Institute of Photonics and Quantum Electronics, CH-1015 Lausanne, Switzerland
[2] Institute of Photonics and Nanotechnology-CNR-via del Cineto Romano 42, 00156 Roma, Italy
[3] Laboratoire de Photonique et de Nanostructures, LPN/UPR 20-CNRS, route de Nozay, 91460 Marcoussis, France

Received 15 August 2006, in final form 12 October 2006
Published 14 May 2007
Online at stacks.iop.org/JPhysCM/19/225005

Abstract

This paper describes the progress towards the realization of efficient single-photon sources based on semiconductor quantum dots (QDs), for application in quantum key distribution and, more generally, quantum communications. We describe the epitaxial growth of QD arrays with low areal density and emitting in the telecom wavelength range, the nanofabrication of single-QD structures and devices, and their optical and electro-optical characterization. The potential for integration with monolithic microcavities is also discussed.

(Some figures in this article are in colour only in the electronic version)

1. Introduction

In the last few decades, scaling down the physical dimensions of electronic devices has been at the heart of the exponential growth [1] of semiconductor electronics: reducing device size allows a higher level of integration and therefore reduced fabrication cost. At the same time, the number of electrons used to encode a single bit in transistors and memories has decreased proportionately to the device area, which obviously allows higher speed and reduced power consumption. The ultimate limit to this trend is represented by single-electron transistors and memories, where a single charge or spin produces measurable changes in the characteristics of a nanoscale device. The very same criteria also apply to optoelectronic devices. The invention of the semiconductor laser, and the subsequent progress in size reduction (single-mode lasers, vertical-cavity surface-emitting lasers (VCSELs), etc) and integration of functionality at the chip level (modulation, amplification, wavelength tuning, etc) have been among the key factors for the development of modern optical communication systems. The example of VCSELs is illustrative: a laser with active volume of few μm^3 provides extremely low threshold currents and low fabrication cost due to small area consumption and wafer-scale fabrication and testing.

Moreover, the steady increase in bit rate has reduced the total energy transmitted per bit—or equivalently the number of photons used to encode the information. In analogy to single-electron transistors, the ultimate limit is given by single-photon devices and single-photon optical communication. While single photons cannot be envisaged for conventional telecom applications, where channel loss would produce unacceptable bit error rates, other applications have emerged which take advantage of the quantum nature of single-photon states.

In particular, quantum cryptography (or more precisely quantum key distribution, QKD) allows unconditionally secure exchange of cryptographic keys by the transmission of optical pulses each containing no more than one photon (see [2] for a review). Eavesdropping can be easily detected since an unknown quantum state cannot be measured without perturbing it—and duplication is forbidden by the no-cloning theorem [3]. Present QKD systems rely on the transmission of strongly attenuated laser pulses, containing an average number of photons $\ll 1$. The probability P_2 of having two photons in a single pulse can in fact be made arbitrarily small by reducing the mean photon number $\bar{n}$: $P_2 = \frac{\bar{n}^2}{2}\mathrm{e}^{-\bar{n}}$ (assuming the Poisson statistics for laser output). The upper limit on the information gathered by an eavesdropper can then be estimated, and a completely secure key can be established by privacy amplification [2]. However, the presence of multiphoton pulses, combined with detector noise and channel loss, imposes a stringent limit on the maximum transmission distance [4], at present of the order of 50–100 km. Moreover, reducing the mean photon number to keep the multiphoton probability small also reduces the number of pulses containing one photon ($P_1 = \bar{n}\mathrm{e}^{-\bar{n}}$), and thus the net key exchange rate (typically to below 1 kb s^{-1}). In contrast, the use of a 'true' single-photon source, i.e. a light source emitting exactly one photon per pulse ($P_1 = 1$, $P_{n>1} = 0$), would circumvent these problems and allow an increase of the QKD channel length and/or of the key exchange rate. However, the realization of such a source requires a change in the photon number statistics from the Poisson statistics of laser light to a highly non-classical statistics where the photon number is perfectly defined—something very different from simply attenuating the laser output. Single-photon pulses can be obtained by exciting single quantum systems—such as single atoms or molecules: an atom pumped to an excited energy state relaxes to the ground state by emitting a single photon—it has to be re-excited to emit another photon. Single-photon generation from atoms [5] and molecules [6] has been demonstrated; however it is in practice difficult to isolate and efficiently collect light from a single atom. Solid-state systems are clearly required for any practical application. Single semiconductor quantum dots (QDs) are promising candidates for such application. QDs are nanosized islands of low bandgap semiconductor in a higher bandgap matrix (e.g. InAs in GaAs). They can be conveniently formed by strain-driven self-assembly in conventional semiconductor epitaxy systems. The electronic confinement (the islands are typically few nm high and 20–30 nm wide) results in a discrete energy spectrum, and in strong carrier correlation effects, making the energy of each electronic configuration (excitons, biexcitons, multiexcitons) easily distinguishable. While each QD can in practice contain several excitons, and will thus emit several photons after the excitation, by spectrally isolating the photon emitted by the last exciton a single-photon pulse is obtained [7–9]. Single-photon emission from self-assembled QDs under optical pumping has been demonstrated mostly in the near-infrared (up to $\approx$1000 nm), at temperatures up to 135 K [10]. Electrically pumped single-photon emitters have been demonstrated [11–14]. First demonstrations of QKD using single-photon sources have also been reported [15, 16].

Overall, while the physical basis for single-photon emission from single QDs seems well established, the technology of practical single-photon devices is still in its infancy. In particular, for practical applications in QKD an emission wavelength of 1300 or 1550 nm is required, which poses significant challenges both in the epitaxial growth (need for large and In-rich

QDs) and in the measurement (InGaAs or Ge avalanche photodiodes must be used, with lower quantum efficiency and much higher noise). For these reasons, the few demonstrations of single-photon emission in the telecom bands [17–19] do not yet match the application requirements. An approach to the fabrication of *efficient* single-QD LEDs (particularly integrating microcavities) still has to be demonstrated, and a systematic investigation of the temperature limitations is lacking. In this paper, we present our progress towards a practical, telecom-wavelength single-photon device. In particular, in section 2 we discuss the growth of sparse arrays of QDs emitting at 1300 nm. Section 3 presents the characterization of single QDs at 1300 nm, in particular the spectroscopic signature of excitons, biexcitons and charged excitons, their time-resolved dynamics and the photon correlation properties. In section 4, an approach to the realization of nanoscale LEDs incorporating few QDs, by the use of oxidized current apertures, is presented. Finally, the integration of wavelength-scale, high quality factor photonic crystal microcavities with single QDs is discussed in section 5.

2. Epitaxial growth

In order to generate single photons, it is necessary to selectively excite a single QD, which can be conveniently done only if the areal density is reduced to one or few dots μm^{-2}. Moreover, an emission wavelength of 1300 or 1550 nm (at the operating temperature, typically $<$100 K) and a high radiative efficiency are needed. The combination of these requirements is not straightforward due to the self-assembled growth mode used for realizing QDs with high radiative quality. In this technique, few monolayers of a highly strained material (e.g. InAs) are deposited on a substrate (e.g. GaAs). Due to the excessive strain, the layers cannot grow in a 2D mode, but rather partly relax the elastic energy by forming coherent islands on top of a thin (1–2 monolayers) 2D 'wetting' layer, in the so-called Stranski–Krastanov growth mode. The density, size and In content of the islands can be controlled by the growth temperature and In deposition rate, but are in general strongly inter-related (see e.g. [20, 21]). A common approach for obtaining low dot densities is depositing a thin layer of InAs close to the 2D–3D growth transition ('critical thickness') [22]. But it is in this case difficult to reach 1300 nm emission since this requires large and thick QDs, i.e. a relatively large amount of InAs. Instead, we have used a combination of ultralow InAs growth rate (about 0.002 monolayers (ML) s^{-1}) and capping with an InGaAs layer to obtain at the same time low dot density and long-wavelength emission [23]. The samples were grown by solid-source molecular-beam epitaxy on (001)-oriented undoped GaAs substrates. Both uncapped and GaAs- or InGaAs-capped samples were grown to investigate the role of growth rate on the dot density and emission wavelength, by atomic force microscopy (AFM) and photoluminescence (PL) spectroscopy, respectively. 2.1 monolayers of InAs were deposited at 505 °C to form QDs by self-assembly. The InAs growth rate R was measured from the 2D–3D transition time and was varied in the 0.17–0.001 ML s^{-1} range by changing the temperature of the indium evaporation cell. For samples used for atomic force microscopy (AFM), after InAs deposition, the substrate temperature was immediately cooled down to room temperature, and the QDs kept under an As overpressure before removal from the growth chamber. The top part of figure 1 shows AFM images of QD arrays grown at two very different InAs growth rates, 0.001 and 0.014 ML s^{-1}. The influence of this growth parameter is strong: dot density decreases from 3×10^{10} dot cm^{-2} to approximately 2×10^8 dots cm^{-2} as the InAs growth rate is reduced from 0.17 to 0.0015 ML s^{-1}. Dot density estimations are confirmed by transmission electronic microscopy (TEM) investigations performed on InAs quantum dots capped by a GaAs layer. The decrease of dot density n_S is due to two distinct processes. On one hand, a reduction of the growth rate R enhances the migration length of In adatoms [24, 25]. This leads to a $n_S \propto R^x$ dependence [26] of

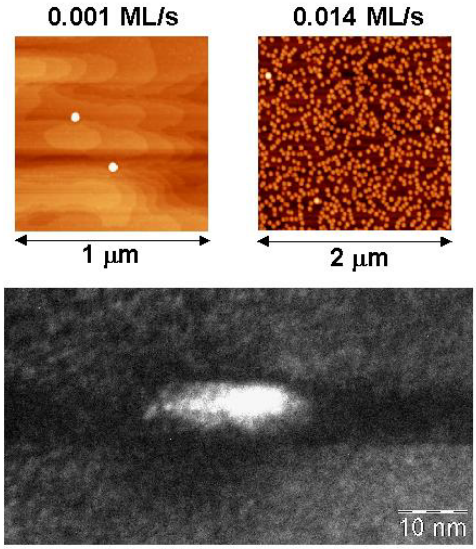

Figure 1. Top: AFM images of QD arrays grown at two very different InAs growth rates, 0.001 and 0.014 ML s^{-1}. Bottom: cross-sectional TEM image ((002), dark field) of an InGaAs-capped QD.

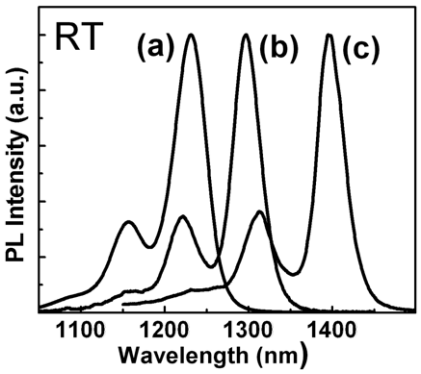

Figure 2. Room temperature PL spectra of (a) high density ($R = 0.016$ ML s^{-1}), (b) low density ($R = 0.0015$ ML s^{-1}) GaAs-capped QDs, and (c) low density ($R = 0.0007$ ML s^{-1}) $In_{0.15}Ga_{0.85}As$-capped QDs.

the areal density and at the same time to an increase in dot size. On the other hand, when the deposition rate is reduced below 10^{-2} ML s^{-1}, In adatom desorption from the growing surface becomes comparable to the deposition rate at this substrate temperature (505 °C), which reduces the number of atoms available for nucleation and produces a sharp decrease in the areal density. Indeed, no 2D–3D nucleation onset was observed below a critical In cell temperature, indicating a limit where the desorption rate equals the deposition rate [27]. Photoluminescence was measured for QD samples grown under the conditions described above and capped by a 100 nm thick GaAs layer. Figure 2 presents room temperature (RT) PL spectra of (a) high density ($R = 0.016$ ML s^{-1}) and (b) low density ($R = 0.0015$ ML s^{-1}) QD ensembles. A red shift of the PL emission wavelength is observed as the growth rate is decreased. This is clearly related to an increase of QD size and/or the In content. The wavelength reaches 1310 nm at RT at the lowest growth rate. In order to further red shift the PL emission, a sample was grown where the QDs deposited at 0.002 ML s^{-1} were capped by a 5 nm thick $In_{0.15}Ga_{0.85}As$ layer followed by 100 nm thick GaAs layer. The InGaAs capping layer reduces the In segregation from the QDs, and results in a larger In content and thus in a red shift of the luminescence. The bottom part of figure 1 shows a cross-sectional TEM image ((002), dark field) of one of these

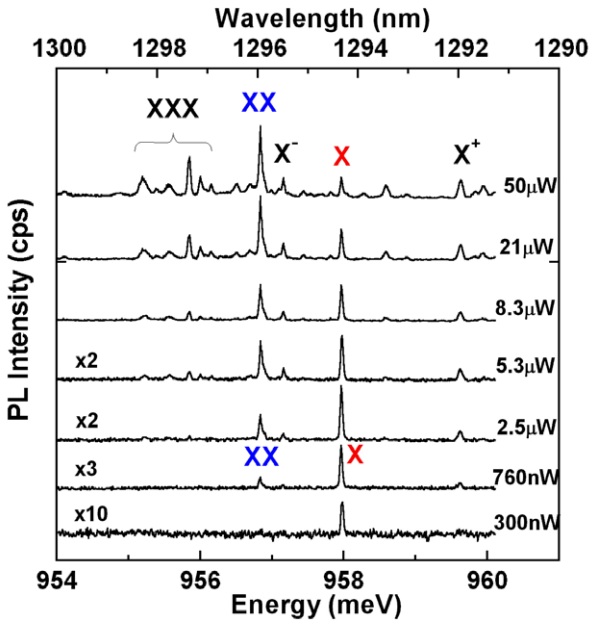

Figure 3. MicroPL spectra of a 1 μm diameter mesa at different excitation powers, showing the emission of a single QD. Peaks X and XX are attributed to exciton and biexciton emission, X^+ and X^- to positively and negatively charged excitons, and XXX to multiexcitons.

InGaAs-capped QDs. Both the dot dimensions (37.5 diameter and 10 height) and the In content (>65% at the QD centre [27]) are far above typical values for InAs self-assembled QDs. PL spectra from this sample are reported in figure 2 (curve (c)), showing a strong PL emission at 1400 nm (RT), which corresponds to 1300 nm at the temperatures (≈10 K) needed for efficient single-photon emission. The combination of ultralow growth rates and InGaAs capping layer thus provides at the same time the dot density and the PL wavelength required for single-photon emission at telecom wavelengths.

3. Optical properties of single 1300 nm QDs

The optimized growth conditions described above allow spectroscopy investigations on single InAs QDs at low temperature. In order to increase the extraction efficiency and thus signal-to-noise ratio, we grew another sample where low density, InGaAs-capped QDs were incorporated at the centre of a 1λ microcavity with a 13.5-pair (1-pair) AlGaAs/GaAs bottom (top) Bragg mirror. This resulted in a 13-fold increase in the collected PL signal close to the 16-fold calculated enhancement of the extraction efficiency in the collection numerical aperture. In order to locally isolate QDs for single-dot spectroscopy, 1 μm diameter mesas were processed by optical lithography and wet etching on the sample with the InGaAs cap layer. The emission from the mesas was measured in a microPL set-up equipped with a microscope objective (numerical aperture 0.5), a grating spectrometer with focal length 1 m and a linear array of InGaAs detectors cooled at 165 K with high sensitivity in the 1000–1600 nm spectral range (see [23] for more details). PL spectra at 12 K obtained for one of these mesas are presented in figure 3 for different excitation powers. Sharp lines are clearly distinguishable, corresponding to the emission of a single QD. Two lines at 957.9 and 956.8 meV can be attributed to exciton (X) and biexciton (XX) transitions, respectively, as evidenced by their excitation power dependence: at very low powers only the X line is present, with a saturation and concomitant rise of the XX line at higher excitation levels. At higher pump powers, other lines appear,

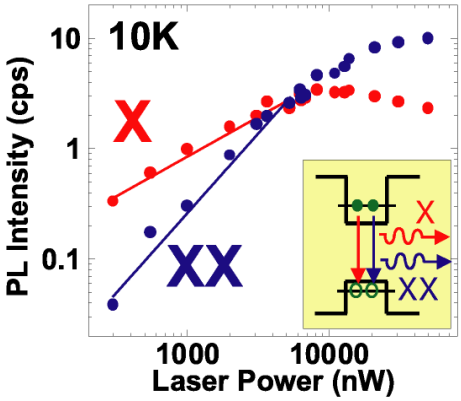

Figure 4. Behaviour of integrated intensities I_X, I_{XX} of X and XX lines as a function of the laser pump power P, under continuous-wave excitation. The lines are fits of $I \propto P^n$ with $n = 0.71$ and 1.4 for the X and XX lines, respectively.

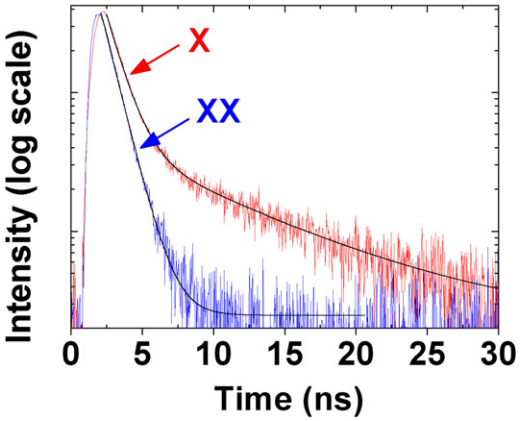

Figure 5. X and XX decay dynamics and corresponding (bi)exponential fits.

which we attribute to charged excitons (X^+, X^-) and to multiexcitons (XXX). Figure 4 shows the variation of integrated intensities I_X, I_{XX} of X and XX lines as a function of the laser pump power P, under continuous-wave excitation. The lines are fits of $I \propto P^n$ with $n = 0.71$ and 1.4 for the X and XX lines, respectively. The fact that the XX line goes as the square of the X line indicates that the emission of a XX photon is related to the probability of having two excitons, and thus confirms the exciton–biexciton character of the two lines.

The time-resolved dynamics of the X and XX emission was investigated by time-correlated fluorescence spectroscopy, using a pulsed diode laser at 750 nm, a Picoquant Time Harp 200 correlation card, and an idQuantique id200 InGaAs single-photon avalanche photodiode (APD). The PL was coupled to a single-mode fibre and the emission of either the X or the XX line was selected with a tunable filter with full width at half-maximum of 0.8 nm. The set-up response function (corresponding to an overall temporal resolution of 600 ps) was measured and then used to fit the decay curves using a single- or double-time constant exponential decay. Figure 5 shows the PL dynamics of the two lines, after dark noise subtraction, together with a biexponential fit (time constants: 1.1 and 8.6 ns) for the X line and a single-exponential fit (time constant: 1.0 ns) for the XX line [19]. The fast time constants are related to radiative recombination of bright states and are consistent with the values measured on shorter-wavelength QDs. The 8.6 ns time constant on the exciton line suggests the presence of a dark exciton state which repopulates the radiative state, as observed for other types of QD [28]. It should be noted that the fast decay of QD states in principle allows a relatively high repetition

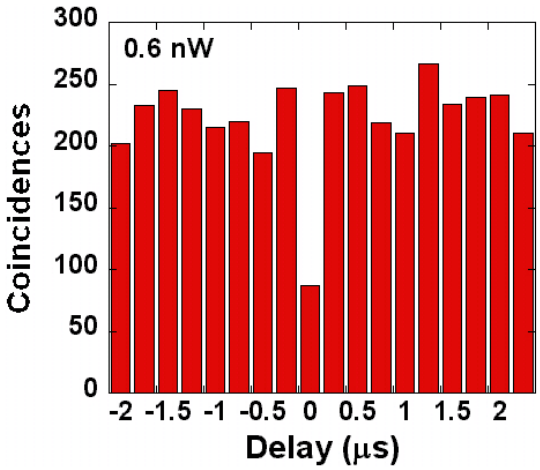

Figure 6. Coincidence counts on the X line as a function of delay for a pump power of 0.6 nW.

rate (at least tens of MHz) of the single-photon source. The decay can be further shortened by integrating an optical microcavity around the QDs.

We then investigated the second-order autocorrelation function $g^{(2)}(\tau)$ of the light emitted by the QD exciton, to assess its suitability as a single-photon emitter [19]. The autocorrelation function at zero delay $g^{(2)}(0)$ for a single-mode field is given by [29]

$$g^{(2)}(0) = \frac{\langle \hat{a}^+\hat{a}^+\hat{a}\hat{a}\rangle}{\langle \hat{a}^+\hat{a}\rangle^2} = \frac{\langle \hat{n}\,(\hat{n}-1)\rangle}{\langle \hat{n}\rangle^2}$$

where $\hat{a}$, $\hat{a}^+$ and $\hat{n}$ are the photon destruction, photon creation and photon number operators, respectively. Indeed, an ideal single-photon emitter produces a Fock state $|1\rangle$ such that $\hat{n}|1\rangle = |1\rangle$ and therefore has $g^{(2)}(0) = 0$ (intuitively, this can be understood as the fact that two photons are never emitted at the same time). In general, $g^{(2)}(0) = (n-1)/n$ for a n-photon Fock state ($n > 1$), while $g^{(2)}(0) = 1$ for Poissonian light. The $g^{(2)}(0)$ is thus directly related to the photon number distribution and represents a figure of merit for application of single-photon sources to quantum key distribution. The $g^{(2)}(0)$ is conveniently measured using the Hanbury-Brown and Twiss experiment where the light is split in two modes 1 and 2 by a 50/50 beam splitter, and two single-photon detectors are placed in the two exit arms. It can then be shown [29] that

$$g^{(2)}(0) = \frac{\langle \hat{n}_1\hat{n}_2\rangle}{\langle \hat{n}_1\rangle\langle \hat{n}_2\rangle}.$$

This allows measuring the autocorrelation function by counting coincidences of detection events on the two detectors. In our experiment (see [19] for more details), the emission of the X line was selected with the filter, and sent to a 50/50 fibre beam splitter and then to two single-photon avalanche photodiodes. Coincidences of detection events were recorded by the correlation card as a function of the delay (in multiples of the laser repetition period). Pulsed operation was imposed by the characteristics of the InGaAs APDs and careful gating of the APDs was necessary to maximize the signal-to-noise ratio (SNR). The histogram of coincidences as a function of delay is shown in figure 6 for a pump power of 0.6 nW (focused on a 4 μm diameter spot size). The $g^{(2)}(0)$ is extracted as the ratio of zero-delay coincidences (proportional to $\langle \hat{n}_1\hat{n}_2\rangle$) and the average of coincidences at multiples of the laser period (proportional to $\langle \hat{n}_1\rangle\langle \hat{n}_2\rangle$, as photons emitted after different laser pulses are uncorrelated).

The lowest measured $g^{(2)}(0)$ is 0.38, which is well below the classical limit of 1, and below the value of 0.5 corresponding to two-photon emission. Nevertheless, $g^{(2)}(0) > 0$, which indicates residual multiphoton emission. A significant fraction of these coincidences are simply due to the limited signal-to-noise ratio of the two detectors—indeed, as noise is classical, it tends to bring the correlation back to the classical value of 1 [30, 31]. In fact, if the measured photon number is the sum of photons emitted by the dot and dark counts, and assuming that the dark counts and signal are uncorrelated, it can be shown that for a perfect single-photon source having $g^{(2)}(0) = 0$, the measured $g^{(2)}_{\mathrm{exp}}(0)$ would be limited by $g^{(2)}_{\mathrm{exp}}(0) \approx \frac{1}{\mathrm{SDR}_1} + \frac{1}{\mathrm{SDR}_2}$, where SDR_i is the ratio of signal counts to dark counts for detector i, assumed $\gg 1$. In the case of the present experiment, the dark count contribution to the $g^{(2)}_{\mathrm{exp}}(0)$ was estimated at 0.14, which brings the source $g^{(2)}(0)$ down to $\approx$0.24. These residual correlations can be attributed in part to stray light not coming from the QD, in part to multiphoton emission from the QD, due to the limited pump pulse width $\approx$50 ps (giving a finite probability of QD re-excitation after photon emission), and to emission from multiexciton states superposed on the X line and thus not adequately filtered. The presence of multiexciton states, presumably related to the presence of carriers in higher energy states, including the wetting layer, is evidenced by a relatively broad PL emission, superposed on the X, XX, and charged X lines, which becomes dominant at high pump power and/or elevated temperature (>50 K) [23]. This stray emission has been observed [32] to increase the $g^{(2)}(0)$ and thus limit the operating temperature of QD-based single-photon sources. Its effect may be reduced by resonant pumping, to avoid generating carriers in the WL, or a careful tuning of the charge state in and around the QD.

4. Single QDs under current injection

For practical applications, single-photon light-emitting diodes (LEDs) would be preferred to optically pumped structures due to the compactness and lower cost. However, controlling carrier injection into a single QD is a formidable task: conventional QD LED and laser structures (see e.g. [33]) typically contain several million QDs. Several approaches have been attempted, such as submicrometre junctions between two crossed wires [34, 35], lateral p–i–n junctions [12] and pyramidal QDs connected by vertical quantum wires [36]. These injection schemes involve complex 3D geometries, and are difficult to integrate with conventional microcavities (based on Bragg mirrors or photonic crystals (PhCs)), which are needed to increase the extraction efficiency. An alternative approach consists of injecting current in a large area, and filtering light from a single QD by the use of a nanoscale aperture in the top metal contact [11]. In this case, although the quantum efficiency (photons/electrons) is very low, a relatively large photon emission probability per current pulse can be obtained ($\approx$5% was demonstrated [13]), as a planar microcavity can be integrated to improve the extraction. The drawbacks are represented by light diffraction at the submicrometre metal aperture, which limits the maximum mode size and therefore the numerical aperture of emission, and the large amount of stray light emitted by the QDs under the metal, which can be coupled to a guided mode and then scattered by the aperture into the collection angle. A more convenient approach would consist of constricting the current injection in a submicrometre area, while keeping a planar structure suitable for integration with microcavities. The use of native Al oxide apertures to confine current injection in submicrometre areas was proposed in [37], and recently exploited by several groups to realize single-QD LEDs [14, 38, 39]. The device structure used by us [39], sketched in figure 7, closely resembles a scaled oxide aperture VCSEL, with a bottom distributed Bragg reflector (DBR), a QD active region, and an AlGaAs aperture layer which is laterally oxidized in a water vapour atmosphere to be transformed into an insulating, low

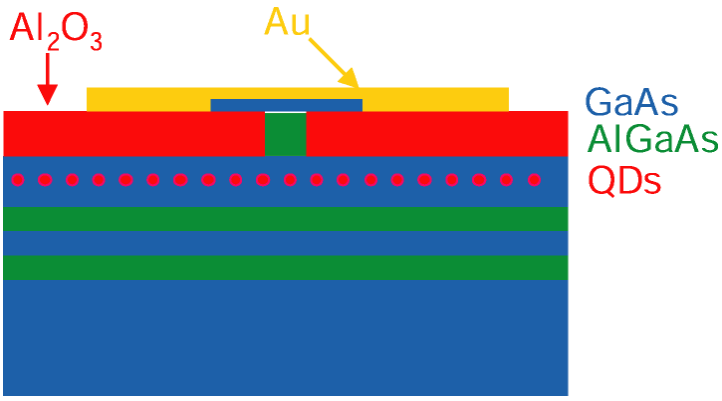

Figure 7. Sketch of a current-apertured nanoscale QD LED.

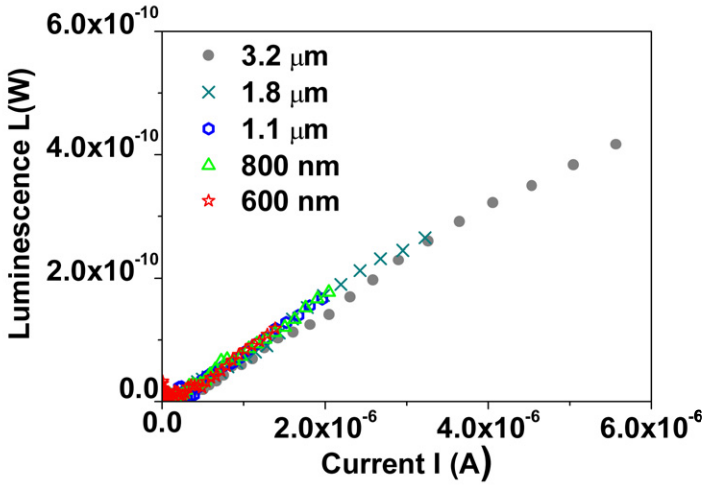

Figure 8. Room temperature electroluminescence of current-apertured LEDs (with a low density QD active region) for different aperture diameters.

index oxide (with a composition close to Al_2O_3). This oxide layer provides at the same time current aperturing and lateral optical confinement. Unlike conventional VCSEL structures, the current injection area must have a diameter well below 1 μm, which requires on one hand a careful processing (control of oxidation time and contact alignment), and on the other hand a stringent control of current spreading (in the layers between the oxide and the QDs) and carrier diffusion in the QD active region. The current spreading can be strongly suppressed by an optimized design of the injection region, while carrier diffusion is fortunately much reduced due to 3D electronic confinement in the QDs [40]. LEDs with this oxide aperture structure and high density QD active regions have shown a nearly ideal scaling of current–voltage and light–current characteristics for aperture diameters down to $\approx$0.5 μm [40]. It has also been observed [39] that the same device structure incorporating low density QDs (1–10 dots μm^{-2}) presents a non-negligible diffusion length of $\approx$1 μm—as evidenced by scaling behaviour—which is due to the larger distance travelled by carriers before being captured in a QD.

Figure 8 shows the room temperature electroluminescence of our current-apertured LEDs, incorporating the low density QDs described in section 2, for different aperture diameters. The efficiency is relatively low ($\eta \approx 10^{-4}$), due to the mismatch in the cavity resonance (the device is designed for optimized extraction at 1300 nm at low temperature), and to the limited RT radiative efficiency in these low density QDs. Nevertheless, the efficiency is independent of

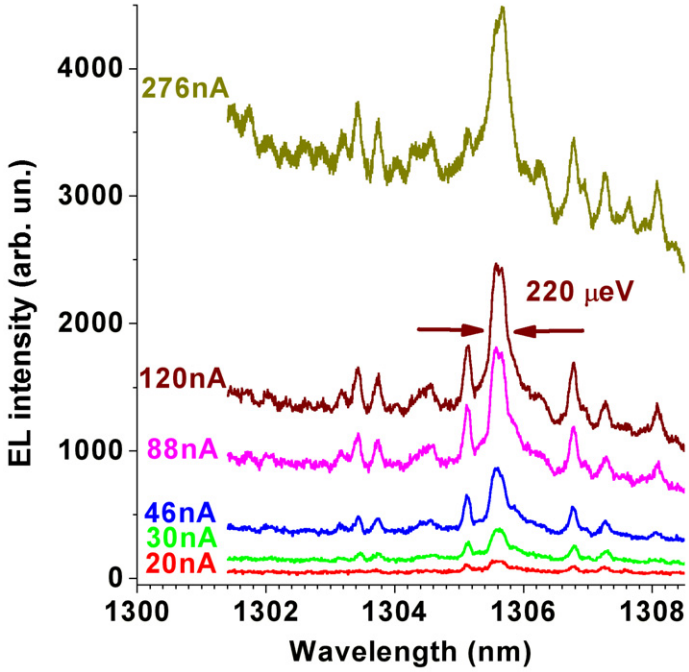

Figure 9. Low temperature electroluminescence spectrum of 2.6 μm diameter current-apertured LED.

the device diameter, implying that no additional non-radiative channels are introduced by the processing.

After bonding and mounting, these devices were tested at low temperatures (10–30 K) [39]. Figure 9 shows an electroluminescence spectrum of a 2.6 μm diameter device for different injection currents. Sharp emission lines appear at low injection levels, which can be attributed to X and multi-X states inside a single QD [39]. This confirms the possibility of injecting current in a single QD by using nanoscale oxide apertures—similar results have also been obtained by other groups [14, 38]. As compared to PL spectra, electroluminescence spectra typically show a larger number of peaks and broad background, which suggests a higher effective temperature at the junction level, and possibly charge states different from those obtained under optical excitation. Further progress, including resonant tunnel injection of cold carriers inside the QD, will be needed to obtain efficient and high purity (low $g^{(2)}(0)$) single-photon LEDs. Integration of electrical injection with micropillars or photonic crystal microcavities is also pursued by a number of groups, to increase the extraction efficiency (see e.g. [41]).

5. Single QDs in microcavities

To have an impact on practical, long-distance QKD systems, QD-based single-photon sources should outperform attenuated lasers and heralded single-photon sources based on parametric downconversion [42], in terms of maximum transmission distance and bit rate. The comparison is made difficult by the fact that security proofs exist only for a limited set of QKD protocols and eavesdropping scenarios. A complete security proof of the Bennett–Brassard BB84 protocol [43], for all individual attacks (attacks on photons one by one) allowed by quantum mechanics has been provided by Lütkenhaus [44], showing a strong impact of multiphoton

emission on the security of QKD systems based on attenuated lasers[4]. In this scenario, single-photon sources start to outperform attenuated lasers for efficiencies (probability of having a photon per pulse) of $\geqslant$ 1%, and show a 10 dB advantage in maximum channel loss for efficiencies of >20% [16]. On the other hand, the much heralded single-photon sources based on parametric downconversion (PDC) [42] provide an interesting alternative to single QDs, with the potential of providing high efficiencies and very low $g^{(2)}(0)$ without the need for cooling. Nonetheless, they typically present a large emission spectrum, with related problems of dispersion in the fibre, while single QDs naturally present a very narrow emission spectrum. The spectral width of PDC single-photon sources can be reduced by filtering, at the expense of efficiency—the competition with single QDs will thus again depend on the efficiency, which can be reached in the two systems for a given $g^{(2)}(0)$ and spectral width. It is thus clear that a possible implementation of QD single-photon emitters in QKD systems is contingent upon the achievement of $g^{(2)}(0) \ll 0.1$ and coupling efficiency of >10% *into single-mode fibres*. The last requirement is extremely challenging, as photons are emitted inside a high index ($n_{\mathrm{GaAs}} \approx 3.5$) medium: assuming for simplicity isotropic emission, 98% of the photons are totally internally reflected at a planar GaAs/air interface, and most of the outcoupled ones are deviated at angles larger than the typical numerical aperture of collection optics (0.1–0.5). The situation can be improved by two approaches:

(a) *Suppress* or reduce spontaneous emission (SE) at angles larger than the critical angle for total internal reflection. This is for instance realized in planar microcavities, where a main Fabry–Perot mode is defined by the two mirrors, with an angle set by the wavelength and cavity length (see [45] for a review). Emission outside the cavity modes is suppressed due to a low optical density of states, which increases the extraction efficiency, i.e. the fraction of outcoupled photons. Planar microcavities have indeed improved the extraction efficiency from single QDs by over a factor of 10 [23]. However, the efficiency of planar microcavities is limited to ≈20–30%, due to 'waveguide' modes propagating parallel to the mirrors, which are not much affected by the mirrors and thus impossible to suppress.

(b) *Increase* the rate of SE into angles which are easily extracted. The SE control is in this case based on the optimization of the optical density of states (by defining a high quality factor mode), and of the quantum mechanical coupling of the emitter to the vacuum field (by defining an ultrasmall mode volume, which corresponds to a larger vacuum field fluctuation). The increase in the SE rate as compared to the bulk value is quantified by the 'Purcell' factor, defined as (see [46] for a review)

$$F_{\mathrm{P}} = \frac{\tau_{\mathrm{bulk}}}{\tau_{\mathrm{cav}}} = \frac{3}{4\pi^2}\frac{(\lambda_0/n)^3}{V_{\mathrm{c}}}Q$$

where τ_{bulk} is the emitter radiative lifetime in a bulk layer, τ_{cav} is the lifetime in the cavity, λ_0 is the vacuum wavelength, V_{c} the mode volume, n the optical index, and Q the cavity quality factor (this expression supposes an ideal situation where the emitting dipole is in spectral resonance with the cavity, placed at the field maximum and polarized parallel to the electric field of the cavity mode). In practice, the difficulty is represented by the contrasting requirements of small modal volume and high quality factor: a high quality factor implies a long photon lifetime, which is difficult to achieve in a small cavity. Microcavities can be monolithically integrated around single epitaxial QDs as micropillars (by etching planar cavities formed by two GaAs/AlAs Bragg mirrors), microdiscs, or membrane photonic crystal (PhC) cavities. The micropillars were first shown [47] to result

[4] We note that this analysis supposes that the eavesdropper can perform quantum non-demolition measurements of the photon number, store photons indefinitely, and control the dark counts of the receiver's detector, three technologies currently not available. The corresponding security conditions are thus perceived as too strict in the QKD community.

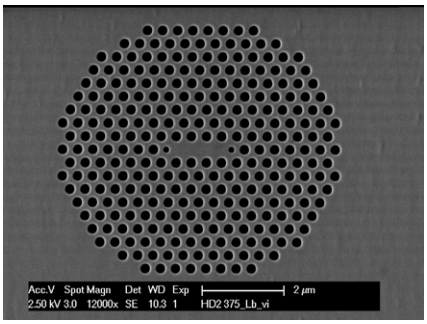

Figure 10. SEM image of an L3-type PhC microcavity where the nearest holes were tuned in diameter and position to increase the Q factor.

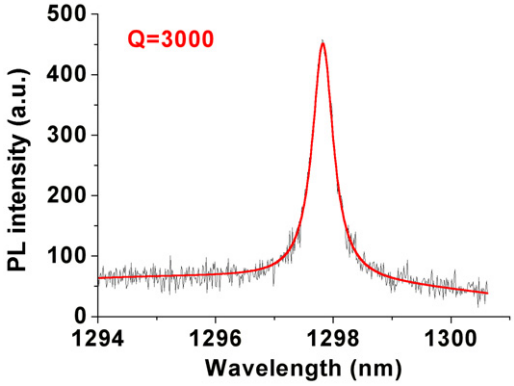

Figure 11. RT PL emission from the L3-type microcavity shown in figure 10, containing high density QDs emitting around 1300 nm.

in a sizable Purcell effect, but more recently SE rate enhancement has been demonstrated also in microdiscs and PhC cavities. The coupling of single QDs to microcavities has also been demonstrated to result in a large Purcell factor and in efficient single-photon emission, both in micropillars [48] and in PhC cavities [49, 50]. PhC cavities at present seem to show the best Q/V_c ratio, and a partially unexplored design potential, due to the possibility of fully engineering the refractive index in a plane (rather than in a single direction, as in the micropillar case).

We have fabricated PhC microcavities in 320 nm thick GaAs membranes. The holes were defined by electron-beam lithography, pattern transfer to a SiO_2 mask, and then reactive ion etching of a GaAs/$Al_{0.7}Ga_{0.3}As$ heterostructure. The GaAs membrane is then released by selective etching of the sacrificial $Al_{0.7}Ga_{0.3}As$ layer. Figure 10 shows the scanning electron microscopy (SEM) image of a modified 'L3' cavity, consisting of a PhC with three missing holes in a row, where the radius and position of the holes next to the cavity centre have been tuned to smooth the mode profile and thus increase the Q factor [51].

In figure 11, the emission spectrum of such a nanocavity containing high density QDs emitting at 1300 nm is reported, showing a cavity mode with a relatively high Q factor of 3000. While these Q/V_c values already allow a strong Purcell effect and efficient single-photon emission [49, 50], even higher Q factors have been demonstrated, up to 1.4×10^5 on GaAs [52] and 10^6 on Si [53], using optimized cavity designs and process technology. In these nanocavities, due to the enhanced exciton–vacuum field interaction, most of SE photons are coupled to the cavity mode. Nevertheless, efficient coupling to single-mode fibres still remains a challenge, as the far-field pattern of high Q modes does not match the fibre numerical aperture. A dedicated PhC cavity design will be required to engineer the free-space radiation

pattern while keeping a large Q/V_c factor. Another approach would be to collect the light *in the plane* of the PhC membrane, i.e. by lateral coupling to a PhC waveguide [54]—this might be easier as in-plane k-vectors are readily controlled by the 2D PhC.

Most work so far has concentrated on self-assembled QDs, whose location and emission energy are random. Coupling with the PhC microcavity is obtained by testing hundreds of structures to find a QD located at the field maximum and spectrally matched to the cavity resonance—fine temperature tuning is then used to bring the QD in and out of resonance. This approach is obviously inefficient and unsuited to mass production. Several researchers are now exploring approaches for controlling the QD and/or the cavity position and energy. For example, growth on pre-patterned surfaces can provide positional control of QDs (see e.g. [55–59]). On the other hand, the PhC cavity can be fabricated *aligned with* a randomly nucleated QD and its resonant frequency matched to the QD emission by post-growth processing [60]. These and similar approaches are expected to provide complete control over the coupling of single solid-state quantum emitters to optical modes—thus providing a powerful tool for investigating and engineering light–matter coupling.

Acknowledgments

We acknowledge financial support from the Swiss National Science Foundation (NCCR Quantum Photonics and Professeur Boursier programmes), the Italian MIUR FIRB programme, EU-FP6 NoE 'ePIXnet' and EU FP6 IP 'QAP'.

References

[1] Moore G E 1965 *Electronics* **38** 114
[2] Gisin N, Ribordy G, Tittel W and Zbinden H 2002 *Rev. Mod. Phys.* **74** 145
[3] Wootters W K and Zurek W H 1982 *Nature* **299** 802
[4] Brassard G, Lütkenhaus N, Mor T and Sanders B C 2000 *Phys. Rev. Lett.* **85** 1330
[5] Kimble H J, Dagenais M and Mandel L 1977 *Phys. Rev. Lett.* **39** 691
[6] Basché T, Moerner W E, Orrit M and Talon H 1992 *Phys. Rev. Lett.* **69** 1516
[7] Michler P, Kiraz A, Becher C, Schoenfeld W V, Petroff P M, Zhang L, Hu E and Imamoglu A 2000 *Science* **290** 2282
[8] Santori C, Pelton M, Solomon G, Dale Y and Yamamoto Y 2001 *Phys. Rev. Lett.* **86** 1502
[9] Zwiller V, Blom H, Jonsson P, Panev N, Jeppesen S, Tsegaye T, Goobar E, Pistol M-E, Samuelson L and Björk G 2001 *Appl. Phys. Lett.* **78** 2476
[10] Mirin R P 2004 *Appl. Phys. Lett.* **84** 1260
[11] Yuan Z, Kardynal B E, Stevenson R M, Shields A J, Lobo C J, Cooper K, Beattie N S, Ritchie D A and Pepper M 2002 *Science* **295** 102
[12] Xu X L, Williams D A and Cleaver J R A 2004 *Appl. Phys. Lett.* **85** 3238
[13] Bennett A J, Unitt D C, See P, Shields A J, Atkinson P, Cooper K and Ritchie D A *Appl. Phys. Lett.* **86** 2005
[14] Ellis D J P, Bennett A J, Shields A J, Atkinson P and Ritchie D A 2006 *Appl. Phys. Lett.* **88** 133509
[15] Waks E, Inoue K, Santori C, Fattal D, Vuckovic J, Solomon G S and Yamamoto Y 2002 *Nature* **420** 762
[16] Beveratos A, Brouri R, Gacoin T, Villing A, Poizat J P and Grangier P 2002 *Phys. Rev. Lett.* **89** 187901
[17] Takemoto K, Sakuma Y, Hirose S, Usuki T, Yokoyama N, Miyazawa T, Takatsu M and Arakawa Y 2004 *Japan. J. Appl. Phys.* 2 **43** L993
[18] Ward M B, Karimov O Z, Unitt D C, Yuan Z L, See P, Gevaux D G, Shields A J, Atkinson P and Ritchie D A 2005 *Appl. Phys. Lett.* **86** 201111
[19] Zinoni C *et al* 2006 *Appl. Phys. Lett.* **88** 131102
[20] Fiore A *et al* 2001 *IEEE J. Quantum Electron.* **37** 1050
[21] Chen J X *et al* 2002 *J. Appl. Phys.* **91** 6710
[22] Leonard D, Pond K and Petroff P M 1994 *Phys. Rev.* B **50** 11687
[23] Alloing B, Zinoni C, Zwiller V, Li L H, Monat C, Gobet M, Buchs G, Fiore A, Pelucchi E and Kapon E 2005 *Appl. Phys. Lett.* **86** 101908

[24] Nakata Y, Mukai K, Sugawara M, Ohtsubo K, Ishikawa H and Yokoyama N 2000 *J. Cryst. Growth* **208** 93
[25] Joyce P B, Krzyzewski T J, Bell G R, Jones T S, Malik S, Childs D and Murray R 2001 *J. Cryst. Growth* **227** 1000
[26] Bartelt M C and Evans J W 1992 *Phys. Rev.* B **46** 12675
[27] Alloing B, Zinoni C, Li L H and Fiore A 2006 unpublished
[28] Patton B, Langbein W and Woggon U 2003 *Phys. Rev.* B **68** 125316
[29] Loudon R 1983 *The Quantum Theory of Light* 2nd edn (New York: Oxford University Press)
[30] Becher C, Kiraz A, Michler P, Imamoglu A, Schoenfeld W V, Petroff P M, Zhang L and Hu E 2001 *Phys. Rev.* B **63** 121312
[31] Brouri R, Beveratos A, Poizat J P and Grangier P 2000 *Opt. Lett.* **25** 1294
[32] Malko A, Oberli D Y, Baier M H, Pelucchi E, Michelini F, Karlsson K F, Dupertuis M A and Kapon E 2005 *Phys. Rev.* B **72** 195332
[33] Fiore A, Oesterle U, Stanley R P and Ilegems M 2000 *IEEE Photon. Technol. Lett.* **12** 1601
[34] Itskevich I E, Rybchenko S I, Tartakovskii I I, Stoddart S T, Levin A, Main P C, Eaves L, Henini M and Parnell S 2000 *Appl. Phys. Lett.* **76** 3932
[35] Schmidt R *et al* 2006 *Appl. Phys. Lett.* **88** 121115
[36] Baier M H, Constantin C, Pelucchi E and Kapon E 2004 *Appl. Phys. Lett.* **84** 1967
[37] Fiore A, Chen J X and Ilegems M 2002 *Appl. Phys. Lett.* **81** 1756
[38] Lochmann A, Stock E, Schulz O, Hopfer F, Bimberg D, Haisler V A, Toropov A I, Bakarov A K and Kalagin A K 2006 *Electron. Lett.* **42** 774
[39] Monat C, Alloing B, Zinoni C, Li L H and Fiore A 2006 *Nano Lett.* **6** 1464
[40] Fiore A, Rossetti M, Alloing B, Paranthoen C, Chen J X, Geelhaar L and Riechert H 2004 *Phys. Rev.* B **70** 205311
[41] Zinoni C, Alloing B, Paranthoen C and Fiore A 2004 *Appl. Phys. Lett.* **85** 2178
[42] Fasel S, Alibart O, Tanzilli S, Baldi P, Beveratos A, Gisin N and Zbinden H 2004 *New J. Phys.* **6** 163
[43] Bennet C H and Brassard G 1984 *IEEE Int. Conf. on Computers, Systems and Signal Processing (Bangalore, India)* (New York: IEEE)
[44] Lutkenhaus N 2000 *Phys. Rev.* A **61** 52304
[45] Benisty H, Neve H D and Weisbuch C 1998 *IEEE J. Quantum Electron.* **34** 1
[46] Gérard J-M and Gayral B 1999 Semiconductor microcavities, quantum boxes, and the Purcell effect *Confined Photon Systems* ed H Benisty *et al* (Berlin: Springer)
[47] Gérard J M, Sermage B, Gayral B, Legrand B, Costard E and Thierry-Mieg V 1998 *Phys. Rev. Lett.* **81** 1110
[48] Pelton M, Santori C, Vuckovic J, Zhang B, Solomon G S, Plant J and Yamamoto Y 2002 *Phys. Rev. Lett.* **89** 233602
[49] Englund D, Fattal D, Waks E, Solomon G, Zhang B, Nakaoka T, Arakawa Y, Yamamoto Y and Vuckovic J 2005 *Phys. Rev. Lett.* **95** 13904
[50] Chang W H, Chen W Y, Chang H S, Hsieh T P, Chyi J I and Hsu T M 2006 *Phys. Rev. Lett.* **96** 117401
[51] Akahane Y, Asano T, Song B S and Noda S 2003 *Nature* **425** 944
[52] Herrmann R, Sunner T, Hein T, Loffler A, Kamp M and Forchel A 2006 *Opt. Lett.* **31** 1229
[53] Asano T, Song B S and Noda S 2006 *Opt. Express* **14** 1996
[54] Gérard J M and Gayral B 2004 *Proc. SPIE—The Int. Soc. Opt. Eng.* **5361** 88
[55] Kohmoto S, Nakamura H, Ishikawa T and Asakawa K 1999 *Appl. Phys. Lett.* **75** 3488
[56] Baier M H, Pelucchi E, Kapon E, Varoutsis S, Gallart M, Robert-Philip I and Abram I 2004 *Appl. Phys. Lett.* **84** 648
[57] Kiravittaya S, Rastelli A and Schmidt O G 2006 *Appl. Phys. Lett.* **88** 43112
[58] Kim J S, Kawabe M and Koguchi N 2006 *Appl. Phys. Lett.* **88** 72107
[59] Atkinson P, Bremner S P, Anderson D, Jones G A C and Ritchie D A 2006 *J. Vac. Sci. Technol.* B **24** 1523
[60] Badolato A, Hennessy K, Atature M, Dreiser J, Hu E, Petroff P M and Imamoglu A 2005 *Science* **308** 1158